atmosphere

MDPI

Article

Preliminary Analysis of Early Identification of Three-Body Scatter Spike Signature in Hailstorms in Catalonia

Tomeu Rigo * and Carme Farnell

Servei Meteorologic de Catalunya, C/Berlin, 38-46, 08024 Barcelona, Spain
* Correspondence: tomeu.rigo@gencat.cat

Abstract: Three-body scatter spike (TBSS) is one of the most common signatures associated with hailstorms using weather radar. It consists of an appendage appearing behind the storms in the radar imagery. The cause is the multi-scattering between hail particles and the ground. The TBSS is detected in plan position indicator (PPI) reflectivity fields at the elevation coinciding with the hail core. Surveillance staff usually analyzes low-level PPI in real-time, but the signature can appear at mid or high elevations. This study takes advantage of the three-dimensional maximum reflectivity (MAX) product for detecting the presence of the TBSS in thunderstorms more easily, instead of the usual way of analyzing the PPI fields. The new technique is more direct and immediate, crucial in real-time surveillance tasks. This preliminary analysis has focused on the hail days with ground registers that occurred in Catalonia between January and August of 2022, observing this signature in the MAX product in 96% of days with large hail and 72% of small hail events. This fact indicates that MAX can be useful for identifying large hail in thunderstorms, but the efficiency decreases for hail smaller than 2 cm.

Keywords: hail; radar; Catalonia; three-body scatter spike; maximum reflectivity field; plan position indicator; vertically integrated liquid

Citation: Rigo, T.; Farnell, C. Preliminary Analysis of Early Identification of Three-Body Scatter Spike Signature in Hailstorms in Catalonia. *Atmosphere* **2023**, *14*, 269. https://doi.org/10.3390/atmos14020269

Academic Editor: Mario Marcello Miglietta

Received: 16 December 2022
Revised: 23 January 2023
Accepted: 27 January 2023
Published: 29 January 2023

1. Introduction

According to Allen et al. (2020) [1], weather radar is the most useful remote-sensing engine for detecting and sizing hail in thunderstorms. The radar variables used are: (1) the reflectivity (horizontal, Z_H, and vertical, Z_V, only on dual-polarization systems); (2) the differential reflectivity (Z_{DR}, the relationship between horizontal and vertical reflectivity, for dual-polarization); and (3) the Doppler velocity estimated in horizontal fields. However, none of these variables, or the combination of some, provides an accurate estimation of the hail size. In any case, there are different methodologies for estimating the hail characteristics in thunderstorms. The techniques include three different categories: direct detection, signatures from explicit variables, and indirect estimation.

There is no direct link between hail size and the observed horizontal reflectivity [1]. This is because the sixth power proportionality between Z_H and the particle's equivalent diameter does not hold any more for hail size larger than 2 cm. Hail size starts to be comparable with typical weather radar wavelengths at S, C, and X bands. However, several experimental and observational studies deduced that rainfall does not produce Z_H over 55 dBZ [1], or at least 50 dBZ [2]. For small hail (<1 cm), [3,4] found that the threshold is 45 dBZ. This threshold is considered an indicator of the presence of hail. However, this does not allow for discriminating between large and small hail [5]. To improve the capability of segregating between different hail sizes (2 cm threshold), the addition of the dual polarization by means of the Z_{DR} to Z_H provides promising results [2,6–8]. However, more research is needed on the dual polarization integration in hail diagnosis. One of the main issues of direct detection methods is the assumption of spherical or spheroid hail shapes, which do not always occur.

The indirect estimation of hail occurrence and size is mainly based on the calculation of the Z_H through each column of the radar volume. In this way, the first estimation consists of the vertically integrated liquid (VIL) [4,5,8], which is an assimilation of the conversion of the horizontal reflectivity in liquid precipitation along all heights. This product has been operational at the Servei Meteorologic de Catalunya to delimitate the affected areas in hailfall cases in agricultural regions [9]. Despite the good results, there are also some limitations (such as the dependence of the VIL threshold throughout the period of the year or the distance of the radar to the region). The VIL density divides the original VIL by the Echo Top of the thunderstorm to consider the vertical development of the cloud. VIL density provides a better estimation of hail presence in thunderstorms throughout all seasons of the year [5,10]. Other indicators consider the exceedance of a Z_H value of an atmospheric level [4,11–13] and some Doppler velocity signatures, such as the divergence at thunderstorm top levels and maximum rotation velocity [1,5]. Farnell et al. [14] presented an acceptable estimation of the hail size in a hailfall event through the combination of radar fields with ground registers using geospatial methodologies. However, a minimum of observations is necessary to work well (one each 10 km^2).

Indirect signatures are those patterns not estimated directly in the radar fields. These signatures, caused by hail in thunderstorms, have been analyzed for detecting and sizing hailstones in real-time surveillance tasks [1]. One indicator is the radar side lobe [15], but the results of using this signature as a diagnostic or forecaster are still preliminary. The well-known signature is the three-body scatter spike (TBSS), defined by [16,17]. The TBSS, or flare echo, consists of a region of large values of Z_H echoes at mid-levels, producing a low reflectivity area with the shape of a spike extending from the core downrange. The physical cause of this signature is still not completely solved, with a dominant theory indicating a contribution of the different scatterings between the hail core, the ground below, and the weather radar [18]. The relationship between the occurrence of hail and TBSS observation seems clear [5,9,11,18], mainly for thunderstorms not farther from the radar than 120 km and with cores at heights between 1200 and 8200 m [19]. Most references agree that the distance to the radar, the size of the region, and reflectivity intensity play a principal role in the size of the TBSS: for those distances to the radar lower than 120 km, with maximum reflectivity over 60 dBZ, and the higher the core area, the more extensive the TBSS [9]. In this way, [18] found that 46% of the analyzed cases had a TBSS. However, there are doubts regarding the TBSS and the hail size [19,20]. It has been detected that weak TBSS patterns in hailstorms produce small sized stones, which could be associated with the dissipating stage of the thunderstorm [19]. For instance, [5] found that the TBSS was detected in 51% of cases with large hail (~5 cm) and 43% of thunderstorms with giant hail (>10 cm). Kumjian et al. [21] observed that the TBSS signature was clearer in polarimetric radar in intense reflectivity cores. Particularly, the best parameters were differential reflectivity and cross-correlation coefficient. Reference [18] indicated that the lead time of the TBSS and the occurrence of hail on the ground does not exceed 30 min. Besides, a principal difficulty of detecting TBSS is that the forecaster needs to analyze the whole set of PPIs, which implies a high time consumption of personal resources that are not always are available in operational meteorological services. Another disadvantage of using TBSS with reflectivity PPIs is that the results are worse than other products, such as radial velocity [18] or storm-relative velocity [11]. However, forecast staff are more commonly adapted to the use of the reflectivity fields.

From the operational surveillance tasks, the forecast team of the Servei Meteorològic de Catalunya has detected some issues related with the identification of the TBSS in real-time. Departing from the premise that the operator has little time for analyzing the radar imagery to diagnose the presence of hail in a thunderstorm and to estimate the probable size of the stones, these issues are the following. (1) The TBSS can be masked by simultaneous and close thunderstorms. (2) The signature can be observed only in mid or high PPI elevations, not typical in those tasks. (3) The TBSS can be masked by electromagnetic interferences [22], anomalous propagation conditions [23], or noise signal (in case of thunderstorms very close

to the radar) because of the low values of the reflectivity in the regions. (4) The signature is not always evident, showing different shapes depending on the nature of the hailstorm, the stage of maturity, or the proximity to the radar, among other elements. To minimize the previous points, the present research considers using the three-dimensional maximum reflectivity (MAX) product for detecting TBSS instead of the PPIs, taking advantage of the fact that this signature is reflected in the vertical cross-sections of MAX. The observations from previous hail campaigns and other analyses such as [24] have led to considering this product for replacing the PPIs. In this way, the use of MAX for detecting the TBSS has been tested in hail events that occurred in Catalonia during the 2022 campaign (from January to August). TBSS observation in MAX consists of a signature over the hail-bearing thunderstorm in some events, like a top hat area of weak reflectivity values observed in the XZ and YZ panels, just over the upper side of the convective cell. Then, we wondered if this signature occurs in most hailstorms. In the case of an affirmative answer, it would help to diagnose the occurrence of hail. The main goals of this preliminary analysis are (1) to investigate the capability of the MAX reflectivity product for identifying the TBSS and (2) to determine the circumstances in which it presents good and bad performance.

The manuscript has the following scheme. First, the document introduces the different radar products used in the study and the methodology considered in each case. The next section presents the obtained results, followed by a discussion of the main elements found. Finally, it ends with the main conclusions of this preliminary analysis of the TBSS observation in the MAX reflectivity product.

2. Materials and Methods

2.1. Data Used

The Radar Network (XRAD) of the Servei Meteorològic de Catalunya consists of four C-Band Single Polarization radars. However, during the period of analysis, only three of the four (PBE, PDA, and CDV in Figure 1) worked in operational mode. There are two scan modes: long (~250 km) and short (~130 km) range. The first one has only one unique elevation (0.6°, the lowest one) and it is used for surveillance purposes. The short-range mode consists of 16 elevations (from 0.6 to 27°) to generate volumetric products. The full scan procedure lasts for 6 min. The data used for this study has consisted of different types of radar products:

- Instantaneous PPI (Plan Position Indicator): The PPI measures the reflectivity and the Doppler velocity fields at each one of the 16 scheduled elevations in a 6-min volume for the closest radar to the hailfall of each day. The coordinates are polar (distance to the radar, azimuth, and elevation) and the resolution is 1 km, 1°, and the 16 elevations. The time resolution is 6 min, and the format of the files is IRIS.
- MAX (maximum reflectivity): MAX provides planar imagery (JPG) of the closest radar to the hailfall. The time resolution is again 6 min, and the spatial resolution is 1 km × 1 km × 0.5 km (cartesian coordinates). The images are composed of three panels, with the maximum reflectivity fields in the X-Y, X-Z, and Y-Z planes.
- VIL (Vertical Integrated Liquid): The VIL is estimated using the classical equation that integrates reflectivity for each layer in the vertical and are an estimation of the precipitable mass water over a pixel. The values range from 0 to 65.5 mm, with 20 mm being a reasonable threshold for hail in our region, according to Rigo and Farnell [19]. The daily fields of the maximum value are in GeoTIFF format, with a spatial resolution of 1 km × 1 km.
- VIL_D (Vertical Integrated Liquid Density): This parameter normalizes the VIL values thorough the division by the echo top (height of the cloud). These normalization results are helpful for obtaining comparable values along the different seasons, and for different vertical developments of the thunderstorms. The values usually move between 0 and 6 mm/km, and 1.5 is a reasonable threshold for hail identification. These have the same attributes as the VIL files.

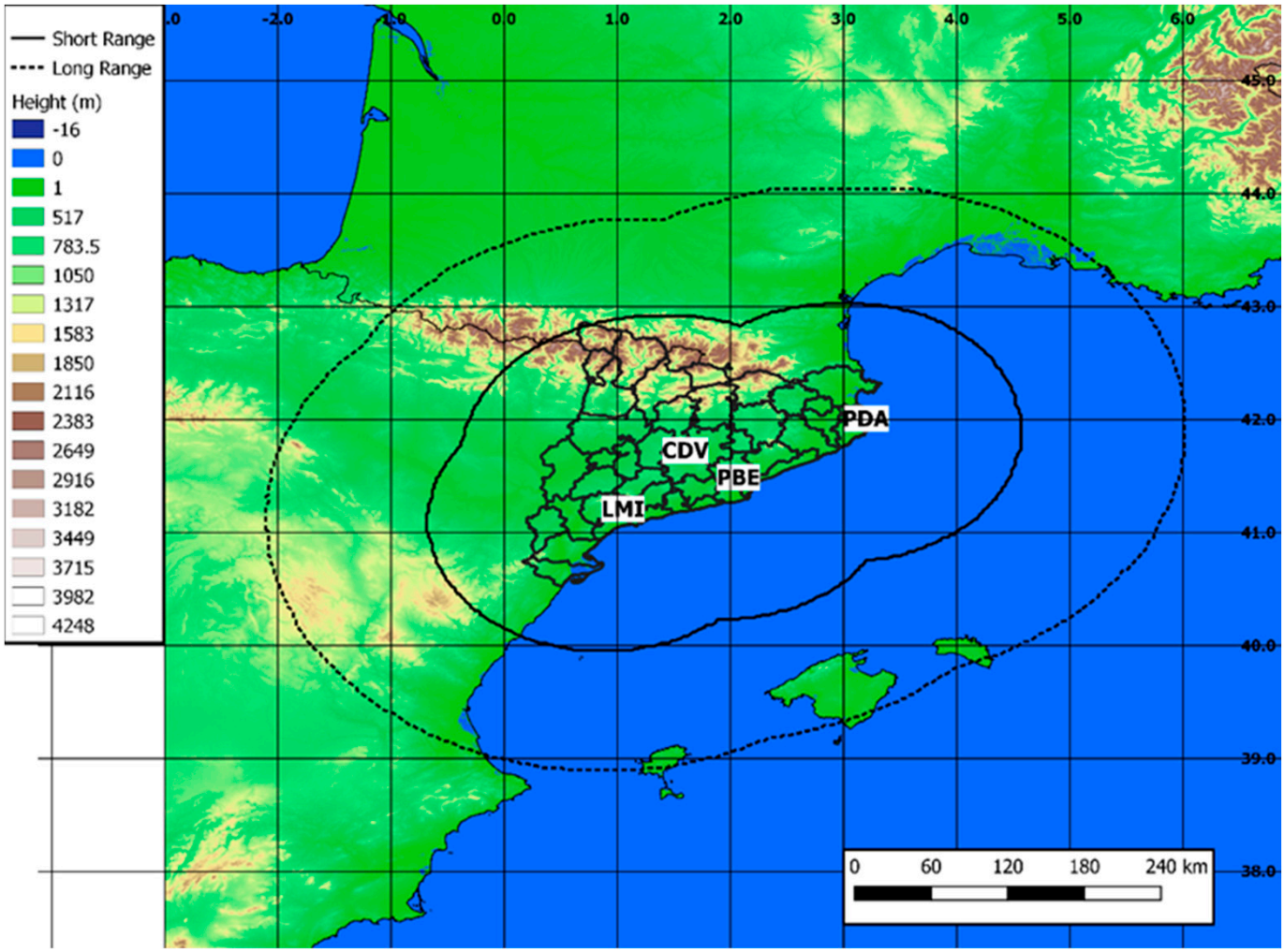

Figure 1. Area of study and the radars of the Servei Meteorologic de Catalunya. The solid and dashed lines indicate the short and long ranges, respectively (see text for more details).

2.2. The Definition of the TBSS in MAX Images

The experience of the Servei Meteorologic de Catalunya staff analyzing hailstorms with radar imagery leads to the identification of a signature in the MAX reflectivity product coinciding with the development and fall of the hail into the cloud. This signature consists of a weak reflectivity (<5 dBZ) region observed in the XZ and YZ panels. The structure goes from the top of the thunderstorm to the top of the radar volume (~20 km A.S.L.) in the vertical of the reflectivity core associated with the hail region. Figure 2 shows an example of a hailstorm affecting the southern coast of Catalonia (1012 UTC on 16 August 2022), observed with the CDV radar (see Figure 1 for the location). The A panel presents the MAX reflectivity product with the signal marked with a blue dashed circle. The B panel is the PPI at 5° elevation for the same time, in which it is possible to observe the "real" TBSS signature. Finally, the C panel is that for the Doppler velocity field at the same time and elevation as the previous one, indicating the high variability observed in the area, associated with the high shear occurring in this type of event.

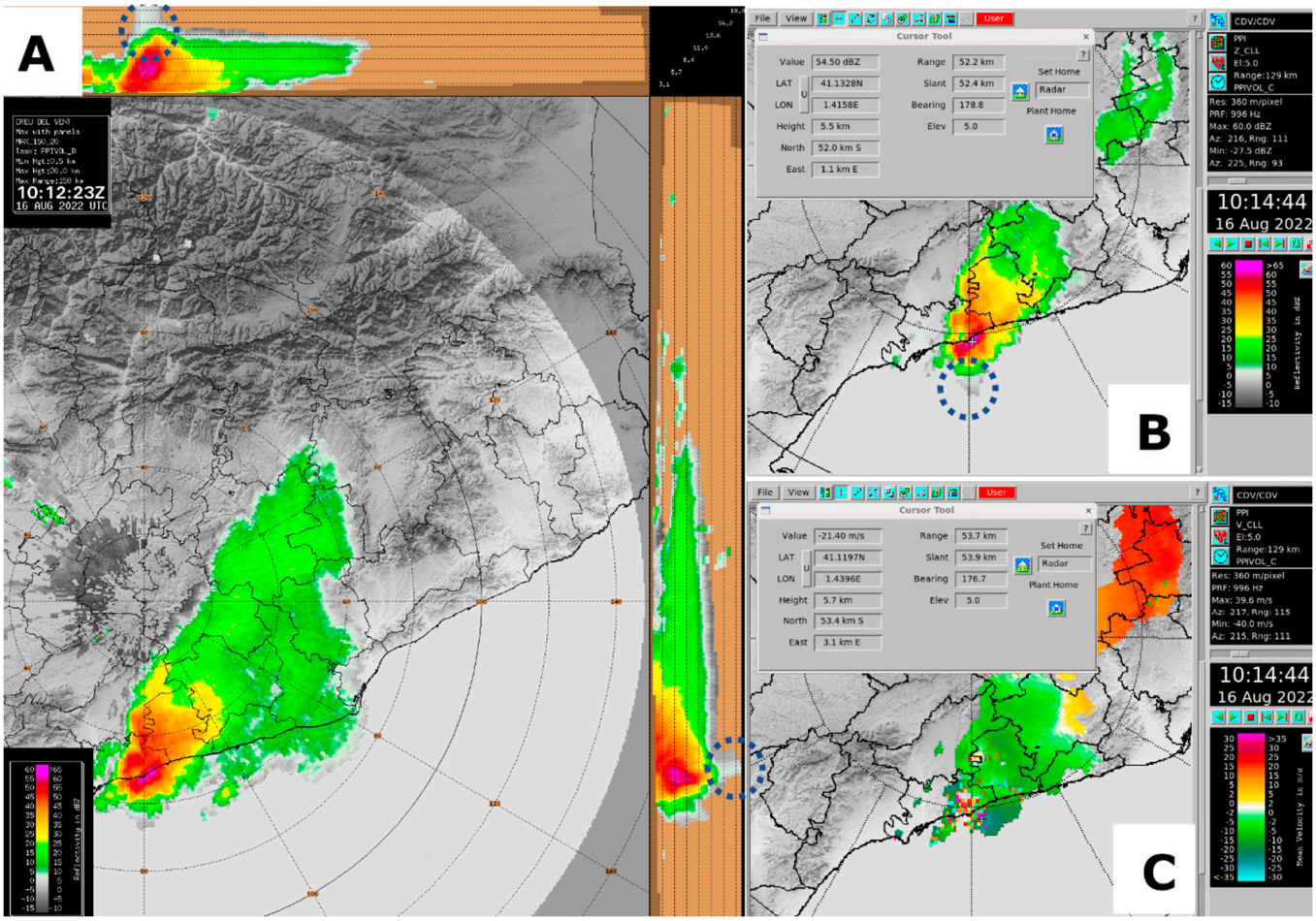

Figure 2. (**A**) Evolution of the MAX reflectivity product at 1012 UTC on 16 August 2022. (**B**) PPI of reflectivity at 5° elevation for the same times as (**A**). (**C**) The same as (**B**), but for the Doppler velocity field. The circles with a dashed blue line in (**A**,**B**) indicate the location of the TBSS.

2.3. Methodology

The research has been divided into three main stages:

1. Identification of days with hail: The selection was made using the hail registers database and the maximum daily VIL and VIL_D radar fields. We used the ground register (that is, observations provided by humans) as the confirmation of hail and to estimate the maximum hail size (we have assumed that the maximum hail size of the event is the maximum observed), while the radar fields were used for estimating the hailfall area. The daily VIL maps were used as the main product, while the daily VIL_D allowed for confirmation of the selected region. Additionally, the 6-min VIL fields helped to confirm the time of occurrence of the hailfall. To validate the characteristics of the TBSS signature, we divided the cases into those with hail of a diameter near 1 cm (small hail) and a diameter larger or equal to 2 cm (large hail). The total of registers was 89: 33 of small hail and 56 of large hail, distributed over 29 days. Figure 3 shows the violin plots of the VIL for the hail register's distributions for each category. The VIL moves between 5 and 65.5 mm (the maximum estimated by the algorithm of the software) in the case of small hail, with a median of 36.5 mm. Opposingly, practically all the values of the VIL for the large hail observations move between 50 and 65.5 mm, with the median close to the latter value.

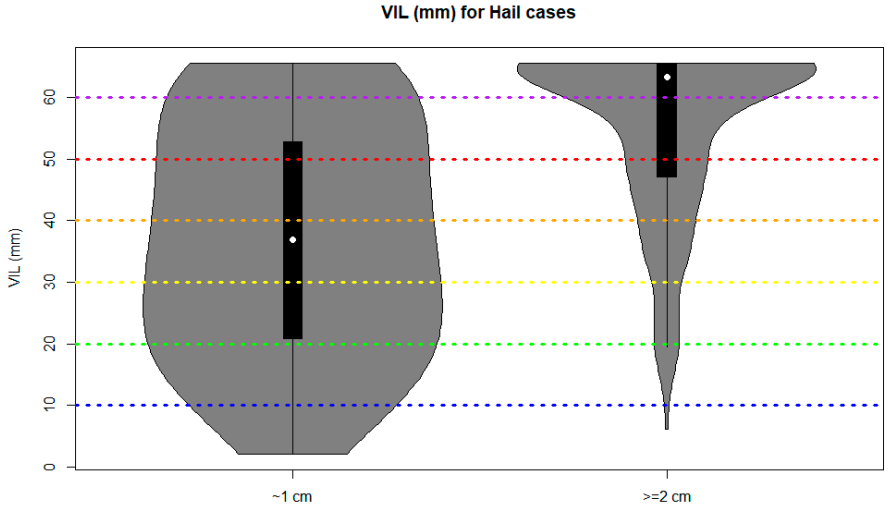

Figure 3. Violin plots for VIL measurements for each of the ground hail registers (**Left**: for hail close to 1 cm diameter, small hail. **Right**: for large hail, equal or larger than 2 cm).

For each hail ground register, we selected the probable area of hail precipitation considering the different factors: the type of event (small or large hail), the month, the distance to the radar, and the area for the different VIL thresholds (this is 20 and 40 mm, similar to [10]). Figure 4 presents two examples of hail events for the two categories (small and large hail), with the area affected by the hailfall.

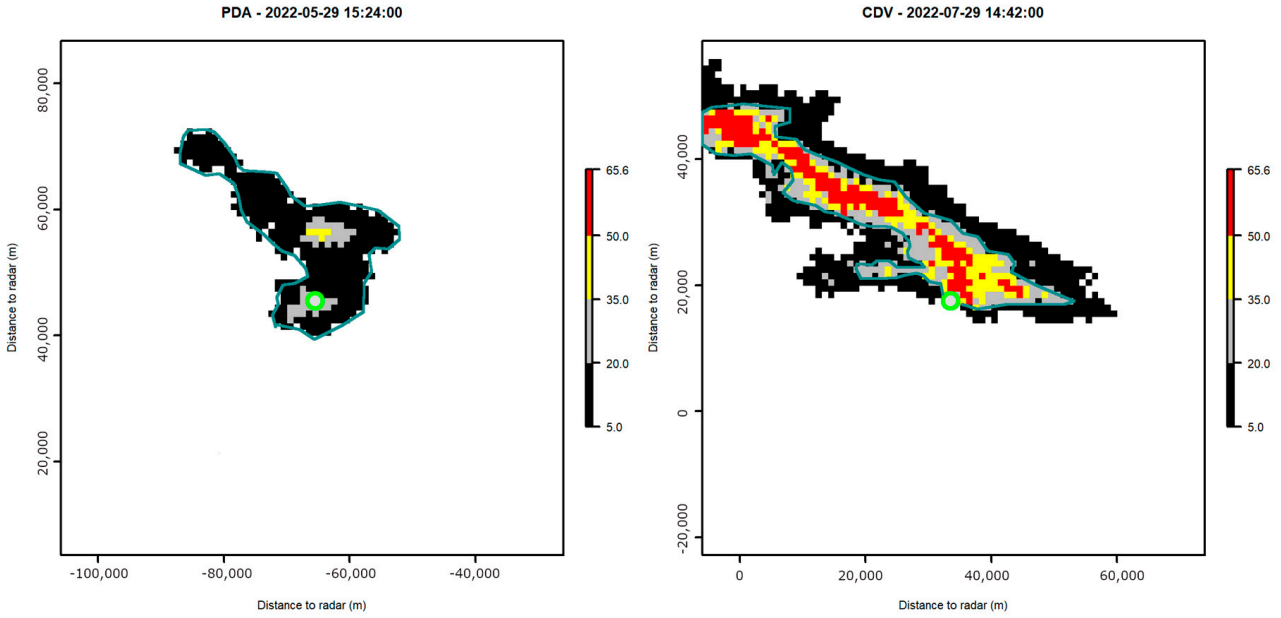

Figure 4. VIL fields for two hail events with different sizes of registers (the green and white dots placed in the centre of each image indicate the location of the register). (**Left**): small hail detected with PDA radar (29 May 2022). (**Right**): large hail detected with CDV (29 July 2022). The cyan line delimitates the hail observed on the ground, according to the criteria of the month, the distance to the radar, the hail size, and the VIL thresholds.

2. Detection of hail cores: Detection consists of the identification of those pixels exceeding the 50 dBZ threshold at each of the PPIs scanned on each of the days selected in the previous phase. Figure 5 shows two examples of the location of the PPI cores centroids (coloured dots) superposed to the VIL area (grey dashed region). The threshold is a bit lower than the one proposed in the bibliography as confirmation of hail. From the authors' experience, the selected threshold is enough for discarding small hail and

graupel cases, but this first analysis focuses on those confirmed events. For each PPI, it selected the region exceeding the threshold, identifying different elements, such as the maximum and mean reflectivity, the height (according to the radar equation), the distance to the radar, the time, and the coordinates.

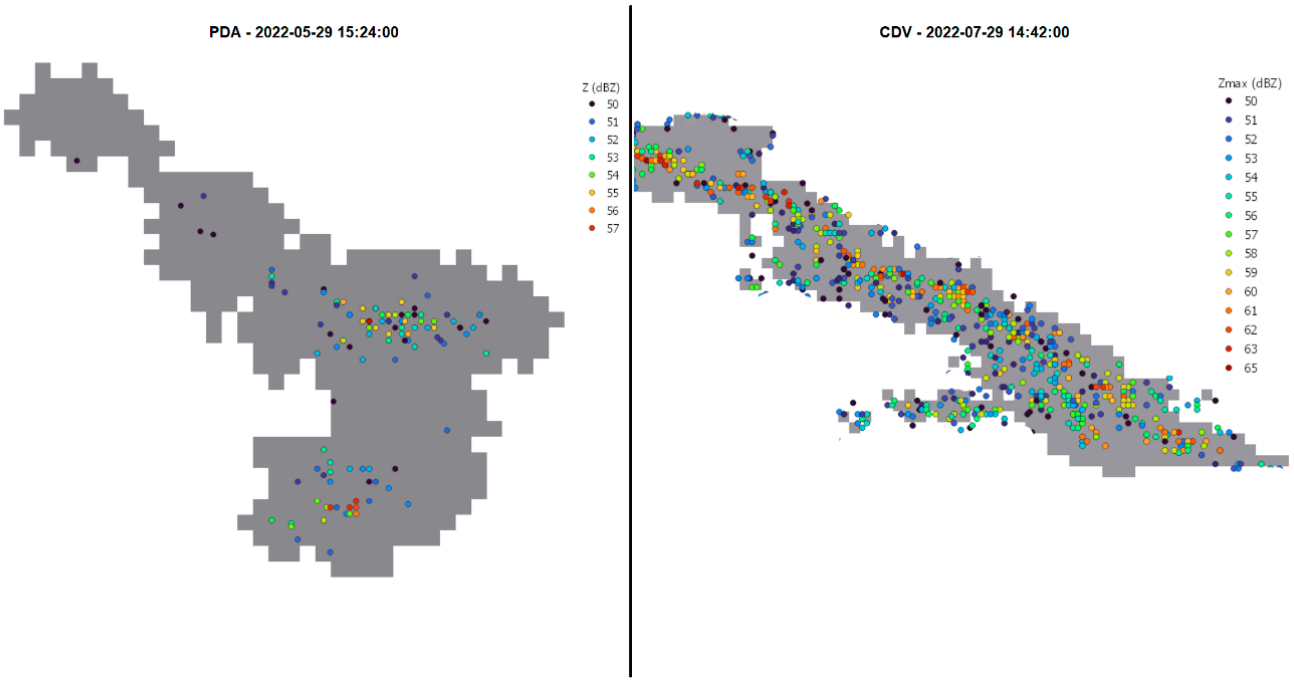

Figure 5. VIL field associated with the hail fall (grey areas) for the same cases shown in Figure 4 (**left**: PDA radar, 29 May 2022; **right**: CDV radar, 29 July 2022). The coloured dots show the locations of the regions exceeding the 50 dBZ threshold for each PPI elevation angle and the colour indicates the maximum reflectivity value.

3. Observation of the TBSS: To verify the occurrence of the TBSS, we have inspected the PPI and MAX imagery in the period between 120 min before and 30 min after the hail ground register has been directly inspected (see examples in Figures 6 and 7). In the case of Figure 7, the TBSS does not appear as in the classical mode, but as a like-a-hat over the thunderstorm top. The analysis includes every 6-min PPI composite and the MAX product with at least one area exceeding the 50 dBZ threshold. First, we searched for the TBSS signature in the PPI composite, selecting those elevations where it was observed. Second, we analyzed the XZ and YZ panels of the MAX product to estimate the vertical profile of the reflectivity in the area with the reflectivity exceeding 50 dBZ.
4. Statistical analysis: To determine the reliability of the occurrence of the TBSS signature in the MAX product, some of the classic skill scores have been estimated using the elements of the measure (Table 1), where the observation is the TBSS occurrence in one or more PPIs, and the forecast is the TBSS detection in the MAX product. The analysis has been made for all the volumes with at least an exceedance of the 50 dBZ threshold.

Table 1. Elements of the measure, forecast, and observation.

Event Forecast	Event Observed	Event Not Observed
Event forecasted	a	B
Event not forecasted	c	D

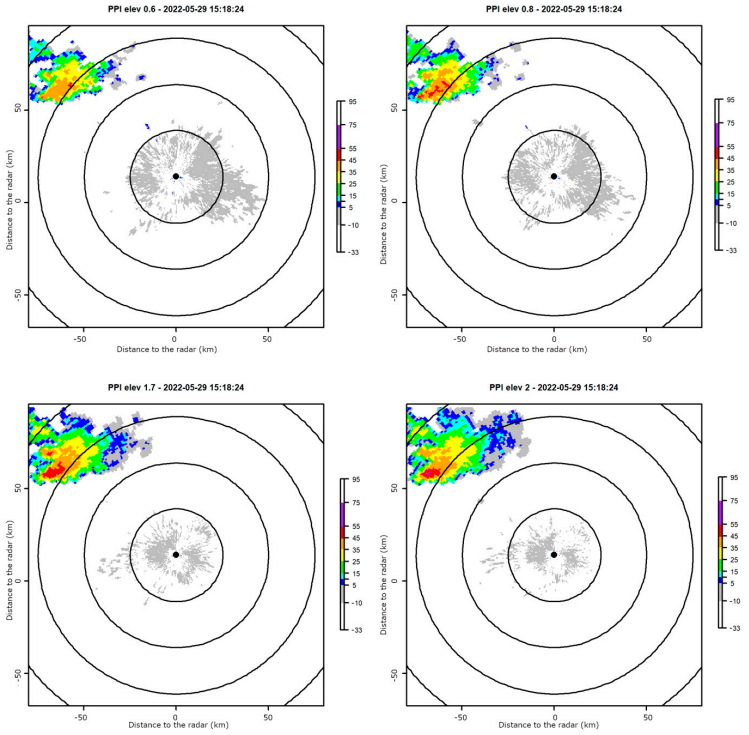

(**A**)

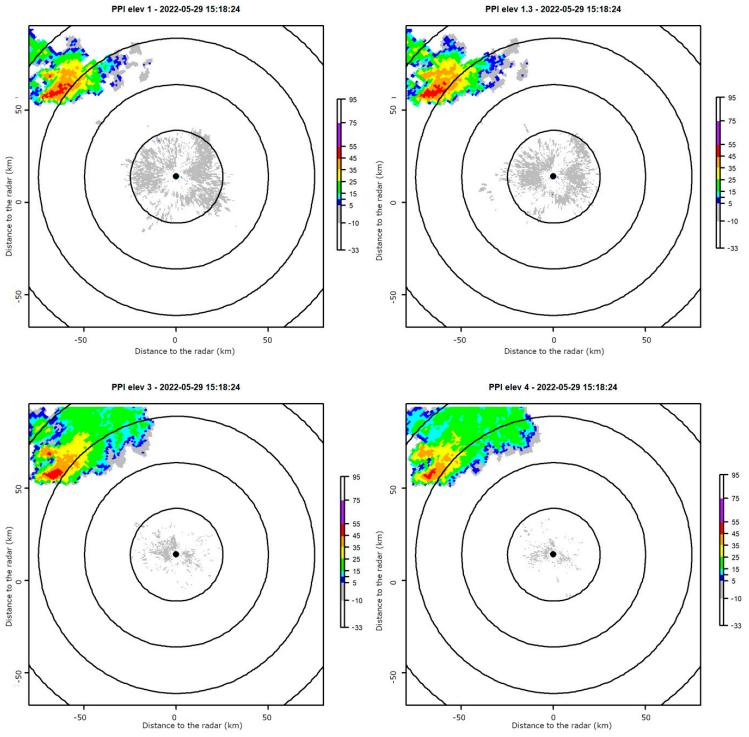

(**B**)

Figure 6. *Cont.*

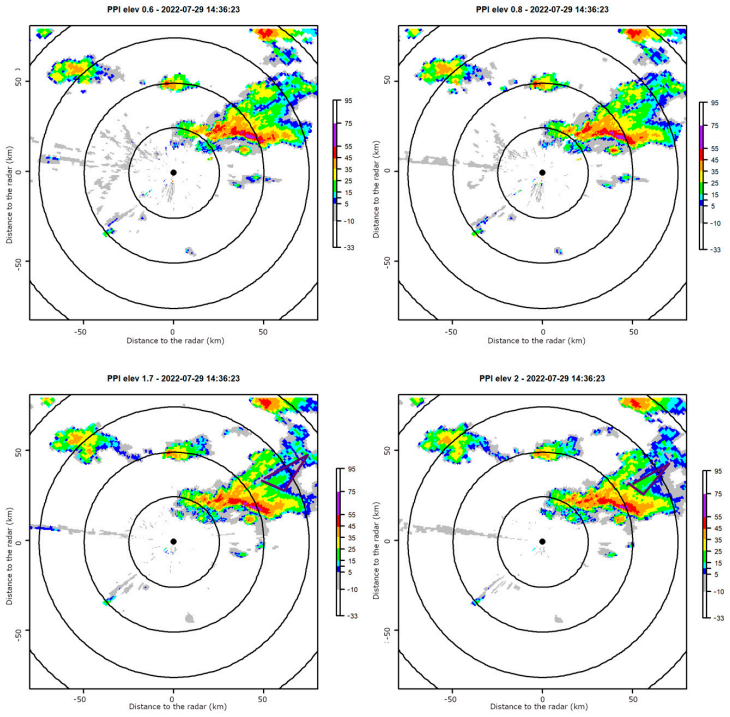

(**C**)

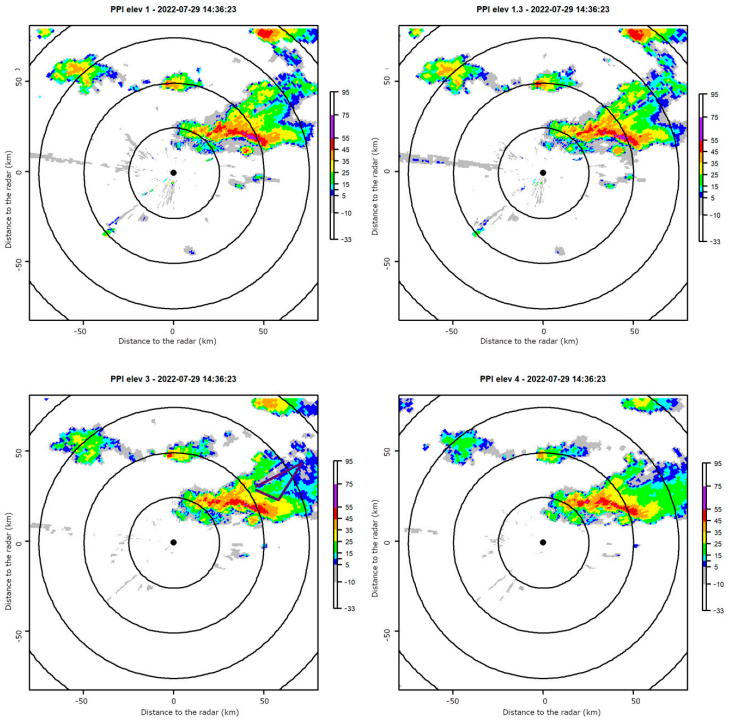

(**D**)

Figure 6. (**A**) Elevations of the PPI fields (0.6, 0.8, 1.7, and 2°) of the same case as Figure 4 (PDA radar, 29 May 2022). (**B**) As in Figure 6A for the 1, 1.3, 3, and 4° PPI elevations (PDA radar, 29 May 2022). (**C**) As in Figure 6A, but for the CDV radar (29 July 2022). The TBSS signature is marked with a purple triangle (in 1.7 and 2° PPI elevations). (**D**) As in Figure 6B, but for the CDV radar (29 July 2022). The TBSS signature is marked with a purple triangle (in 3° PPI elevation).

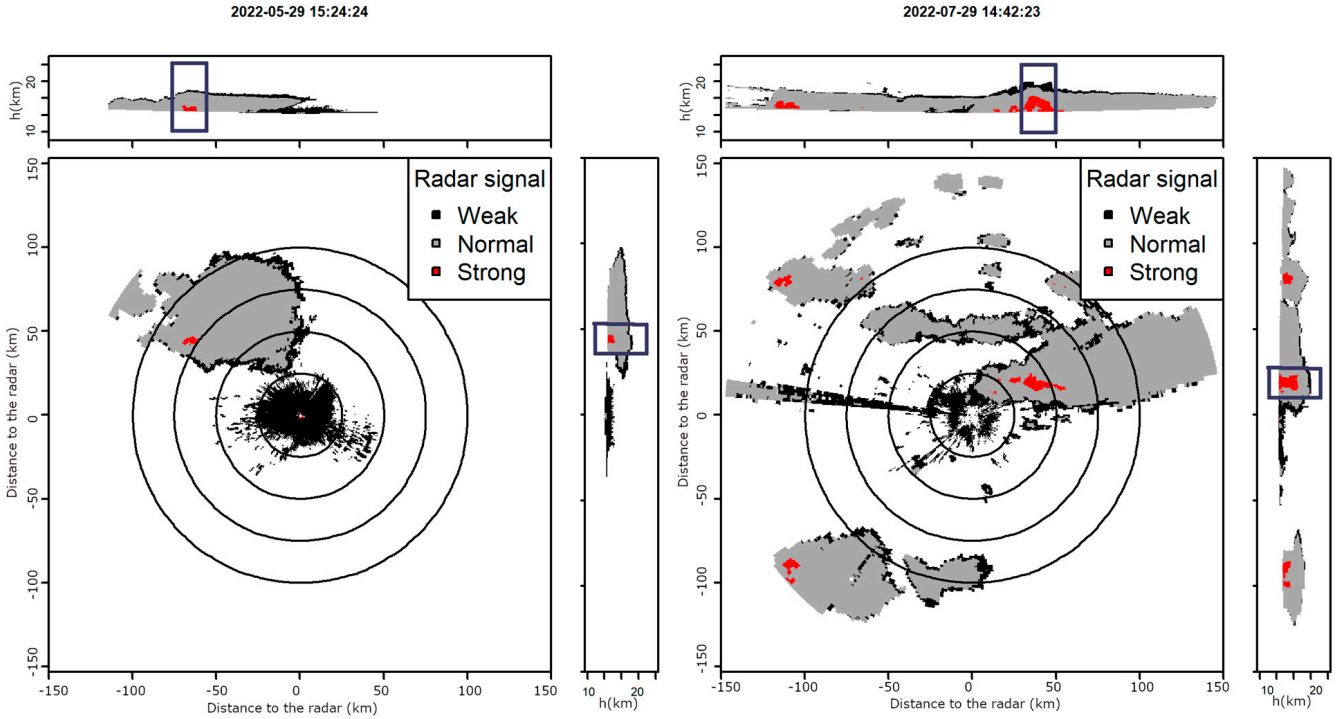

Figure 7. MAX fields of the same cases as Figure 4 (**left**: PDA radar, 29 May 2022; **right**: CDV radar, 29 July 2022). The TBSS signature is marked with a rectangle.

The selected skill scores are the probability of detection, false alarm ratio, and critical success index (Equations (1)–(3)).

$$\text{POD [Probability of Detection]} = a/(a + c), \quad (1)$$

$$\text{FAR [False Alarm Ratio]} = b/(a + b), \quad (2)$$

$$\text{CSI [Critical Success Index]} = a/(a + b + c), \quad (3)$$

3. Results

3.1. Identification of Days with Hail during 2022

The research consists of the analysis of the observation of the TBSS in radar imagery for the hailstorms that produced the 87 ground registers. We divided the cases into two types according to the hailstones' size and following the same method as a previous analysis [25]: small hail, for cases of 1 cm diameter; and large hail, for cases of 2 or more cm. In the first case, May is the month with more registers (9), followed by July, August (7), and April (6). January, March, and June had at least one observation of small hail. On the opposite hand, large hail occurred only in August (38) and July (15). In both cases, the number of hail days was 17, but the mean number of registers was of two per day in the case of small hail and three per day for large hail. The days with more registers were 29 July (12), 21 August (7), 29 May (6), and 30, 27, and 12 August (all three with five registers). There were five days with four registers, three with three registers, and five with two registers. The rest (11) registered only one observation.

This event distribution is consistent with the climatology of the region (see, for instance, [26,27]), with the usual variability of this kind of phenomenon. In any case, the number of days with large hail is a bit larger than the usual, but it is difficult to identify any trend.

3.2. Detection of Hail Cores

The detection of hail cores has allowed for a better identification of the TBSS signature in the next step of the research, for both the PPIs and MAX products, because it indicates the location of the possible candidates. A total of 730 volumes (48.86%) had at least a reflectivity core at any of the 16 PPIs. Of these volumes, 94.24% have registered 16 cores or less. Only 5.75% of the volumes include a thunderstorm with a hail core at all the levels.

To present some of the details of the identified hail cores, Figure 8 illustrates the more representative ones. First, the number of pixels exceeding the 50 dBZ per volume are in the top panel. Most of the cores had very reduced dimensions, especially at high PPI levels. In general, the cores had less than 10 pixels per region. Another factor associated with the size of the cores is the season: larger cores are observed during the warmest months (June to August).

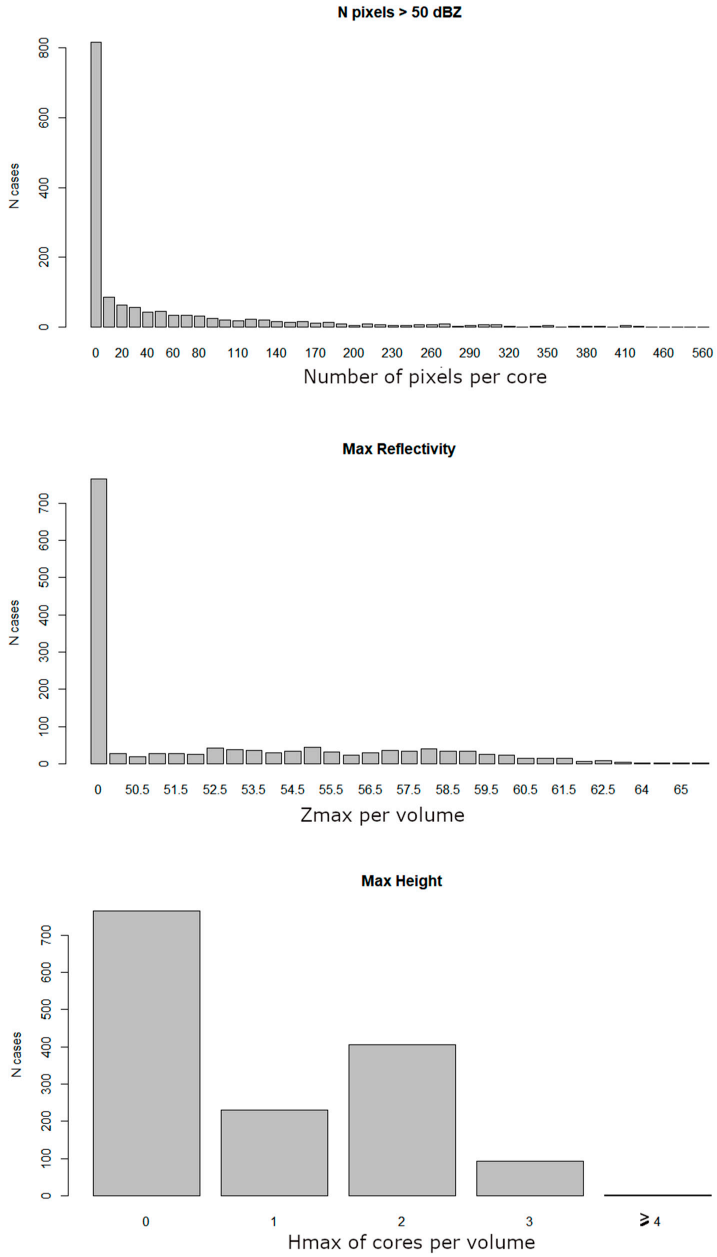

Figure 8. (**Top**): The number of pixels per core. (**Middle**): The maximum reflectivity detected in each volume. (**Bottom**): The maximum height at which the core per volume was detected.

The maximum reflectivity (middle panel of Figure 8) varies from 50 and 65.5 dBZ, but 70.09% range between 53 and 59.5 dBZ, which can be considered as the more common values for this parameter. Again, a high seasonal influence exists in this variable, with the larger values during July and August.

Finally, the bottom panel of Figure 8 presents the highest height of the core, considering that this parameter has been estimated from the radar equation:

$$h = h_0 - r_{ea} + \text{sqrt}(\text{dst}\hat{}2. + 2 \times \text{dst} \times r_{ea} \times \sin(\text{theta} \times \text{pi}/180.) + r_{ea}\ \hat{}2.), \quad (4)$$

where h_0 Vis the height of the radar, dst is the distance of the core to the radar, theta is the elevation angle of the PPI, and r_{ea} is the radius of the Earth. More than the half of the cores were located below 2 km and only few cases exceeded 4 km.

3.3. Detection of TBSS Signatures

First, we have manually analyzed a total of 22,107 PPI fields, corresponding to 1465 radar volumes (each volume is composed of 16 PPIs if the volume is complete). A total of 11,200 PPIs correspond to CDV, 4000 to PBE, and 6907 to PDA (the selection of the radar was made according to the distance of the ground register). For each volume, we identified the number of PPIs where a TBSS signal has been observed. The TBSS signature was observed in a total of 3535 PPIs (15.99%), corresponding to 731 volumes (49.89% of the total of volumes).

Figure 9 shows the distribution of the percentage of PPIs per volume with TBSS signature detection. If each volume has 16 PPIs, then this figure indicates if the signature is easy to detect in the whole set of fields, or, on the contrary, it is usually detected only in a small part of the elevations. As it has been previously stated, half of the volumes included a TBSS. Of this dataset, most of the volumes (a 67.17%) have a third or less than PPIs with the signature, while only a 6.98% have two thirds or more of the PPIs with a TBSS. This means that a TBSS is rarely observed in more than 5 of the 16 PPIs of each volume.

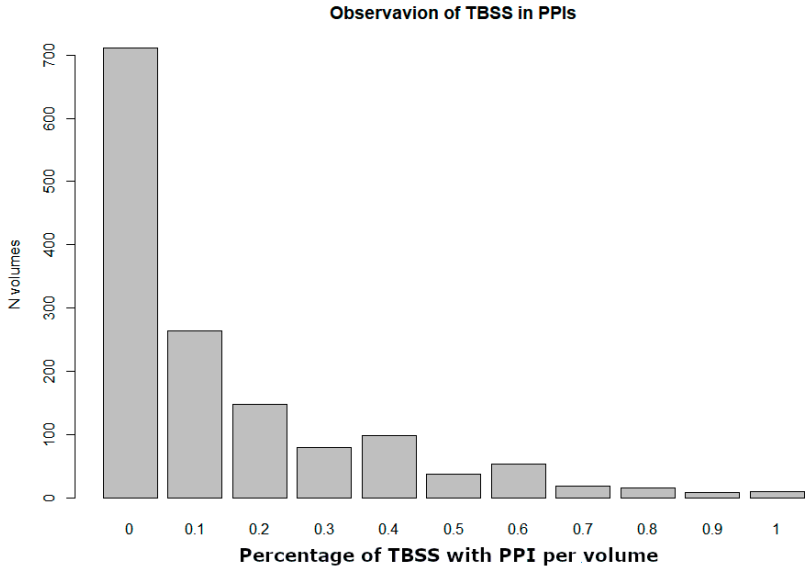

Figure 9. Percentage of PPIs per volume with a TBSS signature.

The signature was also analyzed according to the recorded hail size. In the case of the PPI fields, the signature was identified in 93.94% of the events with small hail, while this percentage is 90.74% for the large hail episodes. Then, the signature was similarly detected for both types of hail size.

The second part of the research consisted of the same type of analysis, but for the MAX products (1442 in total, because the full volume is necessary for generating this product). In this case, the characterization was binary: observation (1) or not-observation (0) of a TBSS

in MAX. In this case, the signature was observed in lower volumes than for the PPIs, with 435 cases, or 30.16% (as it is presented in Figure 10).

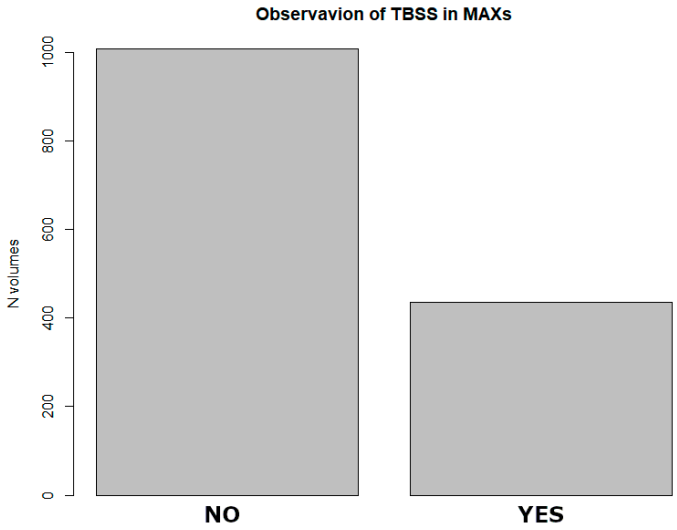

Figure 10. Proportion of MAXs without and with a TBSS signature.

This indicates that this criterium is more restrictive than using PPIs, with some TBSS not identified. However, it is much faster and easier to apply in complex situations. However, there are also some false alarms, because 142 of the signatures corresponded with no signature in the PPIs (19.97% of the total with no TBSS in the PPIs). As the criteria are more restrictive, this increases the percentage of PPIs where the TBSS is detected, and the percentage of identification in the MAX rises: 36.88% of cases when the TBSS is detected in less than one-third of the PPIs of the volume, and 46.21% is the percentage of PPIs that exceeds one-third of the volume.

In the case of the MAX product depending on the hail size register, the TBSS was observed in 57.58% of the events with small hail and 88.89% for the large hail episodes. Unlike the PPIs, the percentage of detection is clearly larger in the case of large hail.

Finally, the seasonal component also plays an important role: the percentage of good observation (that is, observed in MAX and in PPIs) is 6.38% between January and June, while it increases to 48.14% in July and August. This is caused by the fact that the signature is clearer in the warmest months when the convection highly develops.

3.4. Statistical Analysis

The skill scores presented previously (POD, FAR, and CSI) were used to evaluate the quality of the performance of the MAX for identifying the TBSS. We have considered two types of evaluation: first, direct observation of the signature per volume, and second, the same, but for each register (that is, the detection of the TBSS in the 2 **h** before the hail register).

In the first case, the first three rows of Table 2 show the performance of the MAX respective of the PPI for the whole set of volumes, in direct comparison. The values indicate that the capability of directly reproducing the identification of the TBSS with the MAX is of less than half for the whole set, while there is one-third of false alarms. However, these scores vary depending on the season, with clearly worse numbers (lower POD and CSI, and higher FAR) for the colder months (January to June), and much better numbers for the warmer ones (July and August).

Table 2. Skill scores (POD, FAR, CSI) for the global dataset, for the months of January to June, and from July to August.

Period	POD	FAR	CSI
Global	0.40	0.33	0.34
Jan to Jun	0.06	0.63	0.06
Jul & Aug	0.48	0.31	0.40
Small hail (event)	0.72	0.04	0.69
Large hail (event)	0.96	0.02	0.94

However, the interesting use of the signature detection is at the event level, for operation purposes. This means that we are not especially interested in the volumetric detection if the signature has not been detected in the last 2 h prior to the hail register occurrence. In this case, the values are clearly better than for the previous analysis. Again, we divided the dataset in two categories: small and large hail. In the first case, in practically three-quarters of the total cases, the signature was observed in at least one volume prior to the register. This POD is close to 100% in the case of large hail, meaning that the TBSS appeared in practically all the events of large hail. Besides, the FAR is very low (0.04 and 0.02, respectively).

4. Conclusions

The experience in the analysis and observation of hail events in real-time lead to the observation in many cases of a signature in the MAX reflectivity product, which consisted of a vertical structure of weak echoes over the core connected with the hail precipitation in the thunderstorm. The objective of this analysis was to verify the percentage of cases in which the TBSS occurred in the MAX signature. In other words, our goal was to verify if the signature was typical in hail events, and in which cases it occurs more frequently.

To reach the objective, the first eight months of 2022 in Catalonia were analyzed, in which many hail events occurred, most of them with a lot of social interest. Using the VIL and VIL density, the criteria considered in [10], and the registers of the Catalan Hail database [26], the number of cases was 87. To select the hail-producing thunderstorms in each event, the criterium of the 50 dBZ in the reflectivity PPIs at any of the 16 elevations of the more representative radar was used. This criterium is based on the bibliography, and it has a good performance for large hail.

Moving to the results, the vertical weak echo zone in the MAX reflectivity product was usually detected in the events that mainly occurred in July and August. Then, a notable relationship existed between this signature and severe convection, which is the most common type of convection during those periods [28–30]. The comparison with other analyses [1,5,16] or [8] demonstrates that the results obtained are similar with those obtained in this study, clearly detecting the TBSS signature in the MAX product in hail events with a well-defined reflectivity core. These events are associated with hail of a size larger than 2 cm (or severe hail, [26]). Furthermore, this signature is not as clear in events of small hail, coinciding with the findings of [21]. New analyses should also include the height of the reflectivity core [19] or the distance from the radar to the thunderstorm [11].

This preliminary analysis introduces the vertical TBSS as a signature related to hail in events analyzed in Catalonia. This signature would be associated with the TBSS detected in PPI, but in this case, the product used was the MAX reflectivity field. The MAX takes advantage of the capability of representing the reflectivity structure in the atmosphere close to the radar in the different planes (XY, XZ, and YZ).

Although there are some points that need to be investigated more in-depth, the research has led to the main conclusion that the signature effectively reproduces the classical TBSS in severe hail events but is less efficient in small hail cases. The misidentification of cases is contrasted with the faster observation of the signature because the operator can easily identify the signatures using only one image, instead of the difficult analysis of

16 PPIs, in which there is a large set of anomalous reflectivity patterns that can complicate the surveillance tasks.

To end, the conclusions can be summarized as follows:

- We have tested the TBSS signature using MAX in front of a PPI product for the 2022 campaign. During the hail season, large hail only occurred in July and August. The day with more registers was 29 July, but the number of registers per day was higher in August.
- Hail cores detected using PPIs (50 dBZ threshold) are usually small (less than 20 pixels), with maxima reflectivity values between 52 and 60 dBZ, and the height varies between 0.5 and 2 km.
- The TBSS signature usually is observed in two or less PPIs, and rarely in more than two-thirds of the whole volume (16 PPIs). This fact complicates the identification of the signature in real time.
- In the case of the MAX product, the TBSS was observed in 40% of cases where the signature was detected in the PPIs. However, this percentage changes for cold season events (only 6% of detection) and warm season cases (near the 50%).
- If we consider the detection of the signature during a hail event, the percentages of detection are higher, with 72% for small hail and 96% for large hail. This indicates that the MAX can be used properly for large hail identification, while the effectivity for small hail is reduced.

Author Contributions: Conceptualization, T.R. and C.F.; methodology, T.R.; software, T.R.; validation, C.F.; formal analysis, T.R.; investigation, T.R. and C.F.; data curation, T.R. and C.F.; writing—original draft preparation, T.R.; writing—review and editing, T.R. and C.F.; visualization, T.R.; supervision, C.F. All authors have read and agreed to the published version of the manuscript.

Funding: This research received no external funding.

Institutional Review Board Statement: Not applicable.

Informed Consent Statement: Not applicable.

Data Availability Statement: Not applicable.

Acknowledgments: The authors would like to thank their colleagues at the Servei Meteorological of Catalonia for their contributions to the research.

Conflicts of Interest: The authors declare no conflict of interest.

References

1. Allen, J.T.; Giammanco, I.M.; Kumjian, M.R.; Punge, H.J.; Zhang, Q.; Groenemeijer, P.; Kunz, M.; Ortega, K. Understanding hail in the earth system. *Rev. Geophys.* **2020**, *58*, e2019RG000665. [CrossRef]
2. Anderson, M.E.; Carey, L.D.; Petersen, W.A.; Knupp, K.R. C-band dual-polarimetric radar signatures of hail. *Electron. J. Oper. Meteor.* **2011**, *12*, 1–30.
3. Kaltenboeck, R.; Ryzhkov, A. Comparison of polarimetric signatures of hail at S and C bands for different hail sizes. *Atmos. Res.* **2013**, *123*, 323–336. [CrossRef]
4. Paraschivescu, M.; Stefan, S.; Bogdan, M. Verification of an algorithm (DWSR 2500C) for hail detection. *Atmósfera* **2011**, *24*, 417–433.
5. Blair, S.F.; Deroche, D.R.; Boustead, J.M.; Leighton, J.W.; Barjenbruch, B.L.; Gargan, W.P. A radar-based assessment of the detectability of giant hail. *E-J. Sev. Storms Meteorol.* **2011**, *6*, 1–30. [CrossRef]
6. Bringi, V.; Zrnic, D. Polarization weather radar development from 1970–1995: Personal reflections. *Atmosphere* **2019**, *10*, 714. [CrossRef]
7. Picca, J.; Ryzhkov, A. A dual-wavelength polarimetric analysis of the 16 May 2010 Oklahoma City extreme hailstorm. *Mon. Weather. Rev.* **2012**, *140*, 1385–1403. [CrossRef]
8. Montopoli, M.; Picciotti, E.; Baldini, L.; Di Fabio, S.; Marzano, F.S.; Vulpiani, G. Gazing inside a giant-hail-bearing Mediterranean supercell by dual-polarization Doppler weather radar. *Atmos. Res.* **2021**, *264*, 105852. [CrossRef]
9. Rigo, T.; Farnell, C. Using maximum Vertical Integrated Liquid (VIL) maps for identifying hail-affected areas: An operative application for agricultural purposes. *J. Mediterr. Meteorol. Climatol.* **2019**, *16*, 15–24. [CrossRef]
10. Donavon, R.A.; Jungbluth, K.A. Evaluation of a technique for radar identification of large hail across the Upper Midwest and Central Plains of the United States. *Weather. Forecast.* **2007**, *22*, 244–254. [CrossRef]

11. Aran, M.; Sairouni, A.; Bech, J.; Toda, J.; Rigo, T.; Cunillera, J.; Moré, J. Pilot project for intensive surveillance of hail events in Terres de Ponent (Lleida). *Atmos. Res.* **2007**, *83*, 315–335. [CrossRef]
12. Nisi, L.; Hering, A.; Germann, U.; Martius, O. A 15-year hail streak climatology for the Alpine region. *Q. J. R. Meteorol. Soc.* **2018**, *144*, 1429–1449. [CrossRef]
13. Kunz, M.; Kugel, P.I. Detection of hail signatures from single-polarization C-band radar reflectivity. *Atmos. Res.* **2015**, *153*, 565–577. [CrossRef]
14. Farnell, C.; Rigo, T.; Martin-Vide, J. Application of cokriging techniques for the estimation of hail size. *Theor. Appl. Climatol.* **2018**, *131*, 133–151. [CrossRef]
15. Manross, K.L. Examining Radar' side-Lobe Spikes' for Severe Hail Identification. In Proceedings of the 25th Conference on Severe Local Storms, Denver, CO, USA, 11–14 October 2010.
16. Lemon, L.R. The radar "three-body scatter spike": An operational large-hail signature. *Weather. Forecast.* **1998**, *13*, 327–340. [CrossRef]
17. Zrnić, D.S. Three-body scattering produces precipitation signature of special diagnostic value. *Radio Sci.* **1987**, *22*, 76–86. [CrossRef]
18. Carbunaru, D.V.; Sasu, M.; Burcea, S.; Bell, A. Detection of hail through the three-body scattering signatures and its effects on radar algorithms observed in Romania. *Atmósfera* **2014**, *27*, 21–34. [CrossRef]
19. Lindley, T.T.; Lemon, L.R. Preliminary observations of weak three-body scatter spikes associated with low-end severe hail. *E-J. Sev. Storms Meteorol.* **2007**, *2*, 1–15. [CrossRef]
20. Zrnić, D.S.; Zhang, G.; Melnikov, V.; Andric, J. Three-body scattering and hail size. *J. Appl. Meteorol. Climatol.* **2010**, *49*, 687–700. [CrossRef]
21. Kumjian, M.; Picca, J.; Ganson, S.; Ryzhkov, A.; Zrnić, D.S. Three-body scattering signatures in polarimetric radar data. *NOAA/NSSL Rep.* **2010**, *12*.
22. Altube, P.; Bech, J.; Argemí, O.; Rigo, T. Quality control of antenna alignment and receiver calibration using the sun: Adaptation to midrange weather radar observations at low elevation angles. *J. Atmos. Ocean. Technol.* **2015**, *32*, 927–942. [CrossRef]
23. Bebbington, D.; Rae, S.; Bech, J.; Codina, B.; Picanyol, M. Modelling of weather radar echoes from anomalous propagation using a hybrid parabolic equation method and NWP model data. *Nat. Hazards Earth Syst. Sci.* **2007**, *7*, 391–398. [CrossRef]
24. Bocheva, L.; Dimitrova, T.; Penchev, R.; Gospodinov, I.; Simeonov, P. Severe convective supercell outbreak over western Bulgaria on July 8, 2014. *Q. J. Hung. Meteorol. Serv.* **2018**, *122*, 177–203. Available online: http://publications.nssl.noaa.gov/wsr88d_reports/FINAL_TBSS.doc (accessed on 1 December 2022). [CrossRef]
25. Farnell, C.; Rigo, T.; Heymsfield, A. Shape of hail and its thermodynamic characteristics related to records in Catalonia. *Atmos. Res.* **2022**, *271*, 106098. [CrossRef]
26. Farnell, C.; Rigo, T.; Pineda, N. Lightning jump as a nowcast predictor: Application to severe weather events in Catalonia. *Atmos. Res.* **2017**, *183*, 130–141. [CrossRef]
27. Farnell, C.; Rigo, T. The Lightning Jump, the 2018 "Picking up Hailstones" Campaign and a Climatological Analysis for Catalonia for the 2006–2018 Period. *Tethys* **2020**, *17*, 10–20. [CrossRef]
28. Rigo, T.; Llasat, M.C. Forecasting hailfall using parameters for convective cells identified by radar. *Atmos. Res.* **2016**, *169*, 366–376. [CrossRef]
29. del Moral, A.; del Carmen Llasat, M.; Rigo, T. Identification of anomalous motion of thunderstorms using daily rainfall fields. *Atmos. Res.* **2017**, *185*, 92–100. [CrossRef]
30. Rigo, T.; Pineda, N.; Bech, J. Analysis of warm season thunderstorms using an object-oriented tracking method based on radar and total lightning data. *Nat. Hazards Earth Syst. Sci.* **2010**, *10*, 1881–1893. [CrossRef]